

PCCP - Electronic Supplementary Information

Carbon Dioxide and Propane Nucleation: The Emergence of a Nucleation Barrier

Jan Krohn^{a†}, Martina Lippe^{a†}, Chenxi Li^{ab} and Ruth Signorell^{a*}

[†]These authors contributed equally to this work

^aLaboratory of Physical Chemistry, ETH Zürich, Vladimir-Prelog Weg 2, CH-8093 Zürich, Switzerland

^bCurrent Address: School of Environmental Science and Engineering, Shanghai Jiaotong University, Shanghai 200240, China

*Corresponding author: Tel: +41 44 633 46 21, Fax: +41 44 633 13 16, E-mail: rsig-norell@ethz.ch

12

13

14 Formulae for thermodynamic properties

15 We use the expressions for the density (eq. 1) and the surface tension (eq. 2) of liquid C₃H₈
16 and CO₂ given in ref. [1]. The temperature dependence of the vapor pressure of liquid C₃H₈
17 (eq. 3) was also taken from [1], that of solid CO₂ (eq. 4) from [2, 3]. The expression for the
18 second virial coefficients of C₃H₈ and CO₂ (eq. 5) is taken from ref. [4].

$$\frac{\rho(T)}{\text{kg/m}^3} = \frac{A}{B^{1+(1-\frac{T/K}{C})^D}} \quad (1)$$

$$\frac{\sigma(T)}{\text{N/m}} = A \left(1 - \frac{T}{T_c}\right)^B \quad (2)$$

$$\ln \frac{p_{\text{eq,C}_3\text{H}_8}(T)}{p_c} = \frac{T_c}{T} \left[A \left(1 - \frac{T}{T_c}\right) + B \left(1 - \frac{T}{T_c}\right)^{1.5} + C \left(1 - \frac{T}{T_c}\right)^3 + D \left(1 - \frac{T}{T_c}\right)^6 \right] \quad (3)$$

$$\frac{p_{\text{eq,CO}_2}(T)}{\text{bar}} = 10^{A - \frac{B}{T/K - C}} \quad (4)$$

$$\frac{B_2(T)}{\text{cm}^3/\text{mol}} = A + B \frac{10^4}{T/K} + C \frac{10^5}{(T/K)^2} + D \frac{10^9}{(T/K)^3} \quad (5)$$

19 The critical temperatures (T_c) and pressures (p_c) required in (eqs. 2 and 3) are $T_c = 304.3\text{ K}$
20 and $p_c = 73.8\text{ bar}$ for CO₂, and $T_c = 369.9\text{ K}$ and $p_c = 42.5\text{ bar}$ for C₃H₈ [1]. All the other
21 parameters for the above formulae are collected in Table S1. We note the rather high uncertainty
22 of the extrapolation of physical properties to very low temperatures, already discussed in [5].

substance	equation	A	B	C	D
CO ₂	(1)	0.7159007	0.02087	310.668	0.07579
C ₃ H ₈	(1)	0.8485280	0.03267	388.531	0.10439
CO ₂	(2)	0.08167	1.27339	-	-
C ₃ H ₈	(2)	0.05094	1.22051	-	-
C ₃ H ₈	(3)	-6.71791	1.33932	-2.23017	-1.24990
CO ₂	(4)	6.81228	1301.679	3.494	-
CO ₂	(5)	57.40	-3.8829	4.2899	-1.4661
C ₃ H ₈	(5)	109.71	-8.4673	-81.215	-3.4382

Table S1: Parameters for the density (eq. 1) and surface tension (eq. 2) of liquid CO₂ and C₃H₈, for the vapor pressure of liquid C₃H₈ (eq. 3) and solid CO₂ (eq. 4), and for the second virial coefficient (eq. 5) of CO₂ and C₃H₈. The formulae and parameters are taken from refs. [1], [2, 3] and [4].

²³ **Vapor pressure for CO₂ and C₃H₈**

²⁴ The vapor pressure of CO₂ given by the Wagner formula from [1] for the gas-liquid interface
²⁵ (eq.3) shows some lack of agreement with measurements performed by Giauque and Egan [3]
²⁶ (see zoom in in Fig. S1). Based on these measurements Azreg-Ainou [6] (green squares in
²⁷ Fig. S1a) theoretically predicted the vapor pressure at even lower temperatures. Since the
²⁸ results demonstrate the validity of the Antoine equation from NIST [2] at lower temperatures
²⁹ (eq.3), we use it to calculate the vapor pressure of CO₂ at the gas-solid interface. For the vapor
³⁰ pressure of liquid C₃H₈ the situation is reversed: the Wagner formula from [1] (eq.3) agrees well
³¹ with experimental data [7, 8] and theoretical predictions [9] (see zoom in in Fig. S1b), while
³² the Antoine formula (eq.4) shows disagreement with experiments around 90 K. Consequently
³³ we decided to use the Wagner formula from [1] (eq.3) for the vapor pressure of C₃H₈.

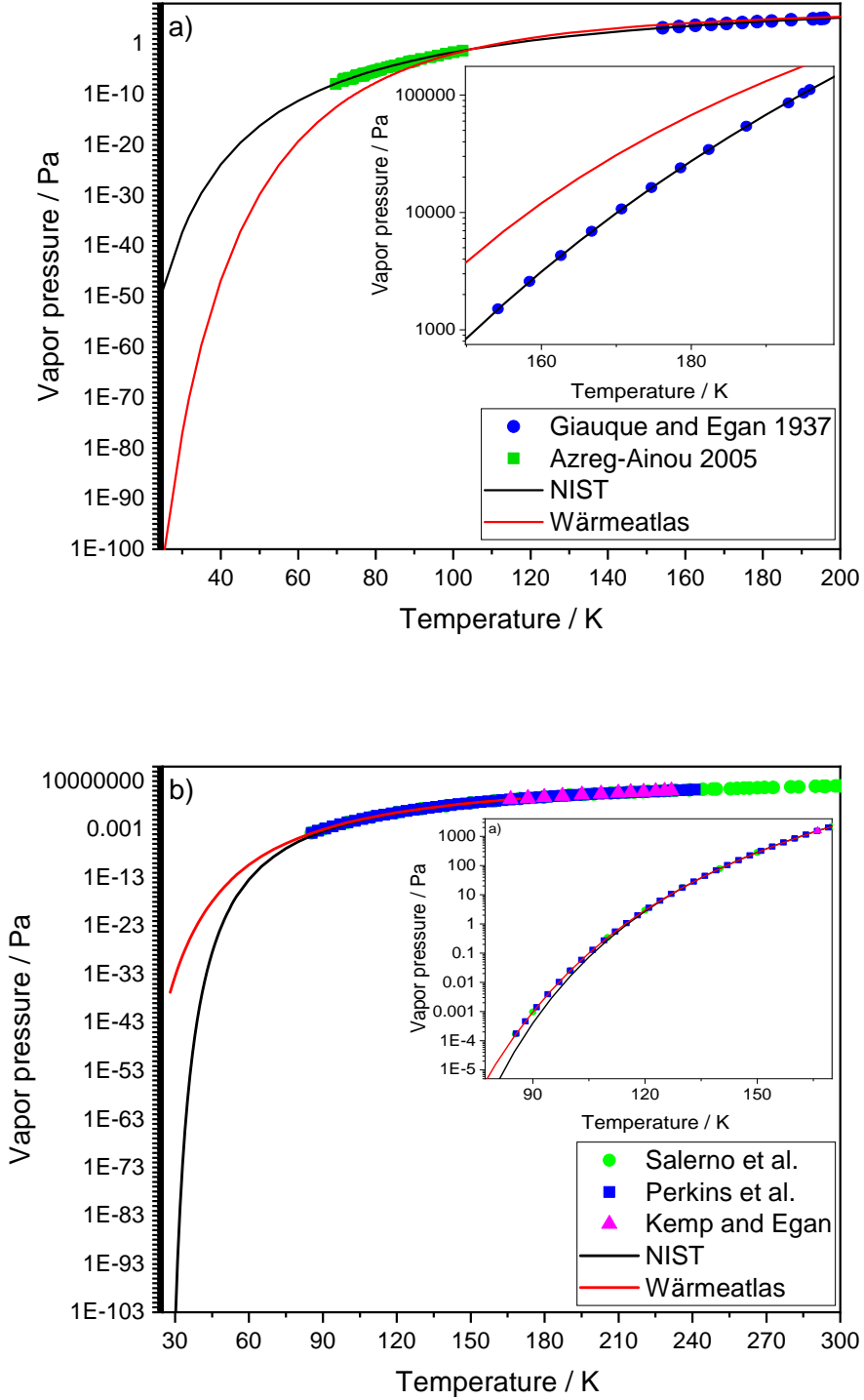
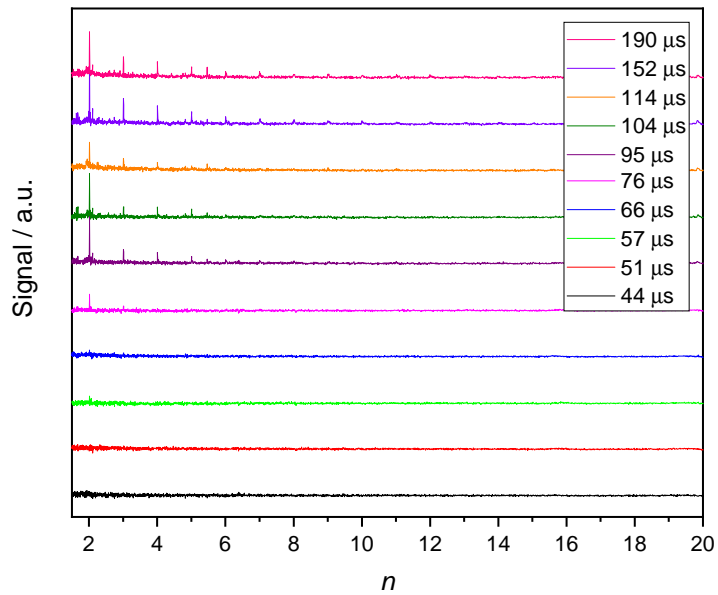


Figure S1: a) Vapor pressure of CO_2 as a function of temperature using the Wagner equation for the gas-liquid interface from [1] (eq.3, red trace) and using the Antoine equation for the gas-solid interface from [2] (eq.4, black trace). Experimental points by Giauque and Egan [3] and predictions by Azreg-Ainou [6] are shown as blue circles and green squares, respectively. b) Vapor pressure of C_3H_8 as a function of the temperature using the Wagner equation from [1] (eq.3, red trace) and the Antoine equation from NIST [2] (eq.4, black trace), both for the gas-liquid interface. Experimental data points from Perkins et al. [7] and Kemp and Egan [8], and predictions from Salerno et al. [9] are shown as blue squares, pink triangles and green circles, respectively.

³⁴ Mass spectra for C₃H₈ nucleation

a) 0.035% C₃H₈



b) 0.26% C₃H₈

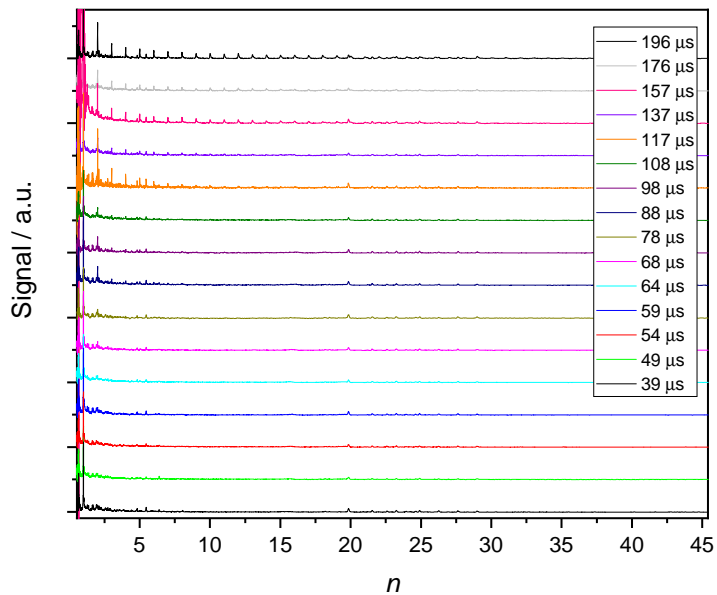


Figure S2: Mass spectra of C₃H₈ given in number of C₃H₈ molecules per cluster n for 0.035% and 0.26% concentration. The Figure is analogous to Fig. 2 for CO₂ in the main part. The signal marked in the range of $n \sim 20\text{-}30$ corresponds to uncompensated background signal.

35 Complete data for the number concentrations as a function of the
 36 time

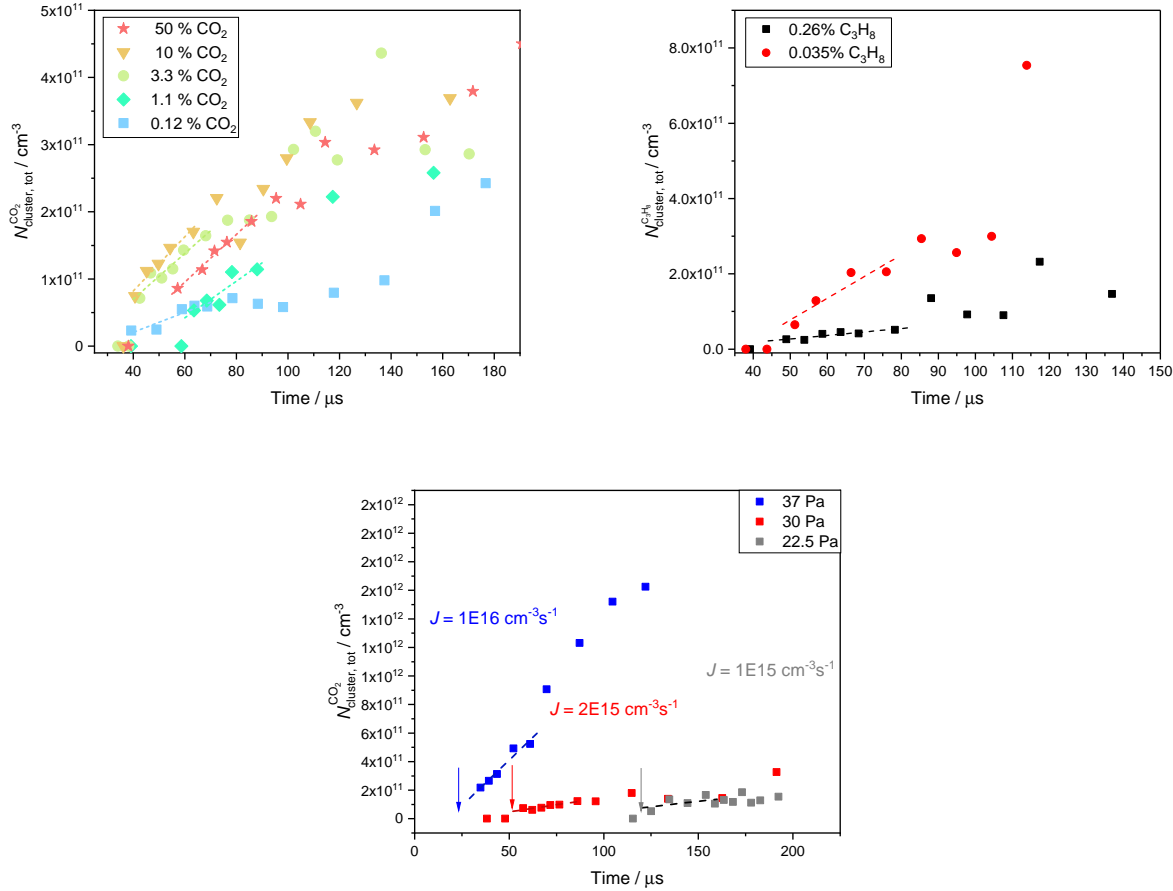


Figure S3: Time evolution of the total number concentrations of CO_2 clusters. a) Dependence on CO_2 concentration (50, 10, 3.3, 1.1 and 0.12%). b) Dependence on C_3H_8 concentration (0.26 and 0.035%). c) Dependence on the total pressure (22.5, 30 and 37 Pa). This Figure is analogous to Fig. 3, Fig. 4 and Fig. 7, respectively, in the main text, where only the points used for the linear fits are shown.

³⁷ **Kinetic model for C₃H₈ and CO₂ data**

³⁸ As discussed in the main text, we construct a net forward rate constant $k_{1j,\text{net}}$ that com-
³⁹ bines the contribution of evaporation and association. The evolution of the monomer number
⁴⁰ concentration N_1 is given by:

$$\frac{dN_1}{dt} = -N_1 \sum_{j=1}^{\infty} (1 + \delta_{1j}) k_{1j,\text{net}} N_j \quad (6)$$

⁴¹ With δ_{1j} being the Kronecker delta and N_j being the number concentration of cluster j . The
⁴² temporal change of the concentration of the clusters with size $j > 1$ is given by:

$$\frac{dN_j}{dt} = (k_{1j-1,\text{net}} N_{j-1} - k_{1j,\text{net}} N_j) N_1 \quad (7)$$

⁴³ Eq. 7 only accounts for cluster growth via the addition of a monomer, since coagulation between
⁴⁴ different clusters is negligible under our conditions [10]. We used eq. 4 in the main text to
⁴⁵ determine the net forward rates $k_{1j,\text{net}}$. We used the model of eq. 6 and 7 to calculate the
⁴⁶ cluster size distribution (red in Fig. S4 and S5) and adjusted $k_{1j,\text{net}}$ by visual inspection to
⁴⁷ match the experimental cluster size distribution (black in Fig. S4 and S5). Examples for CO₂
⁴⁸ and C₃H₈ are shown in the following.

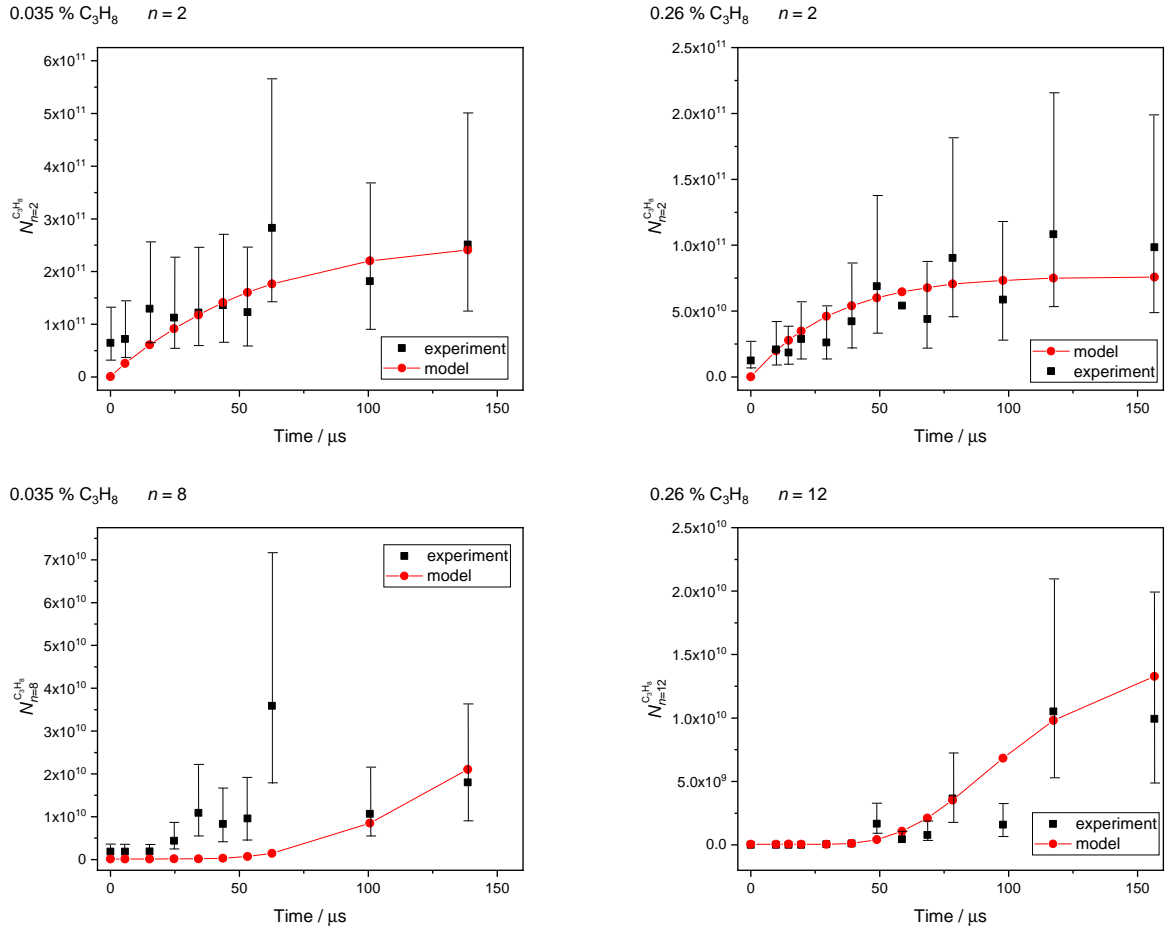
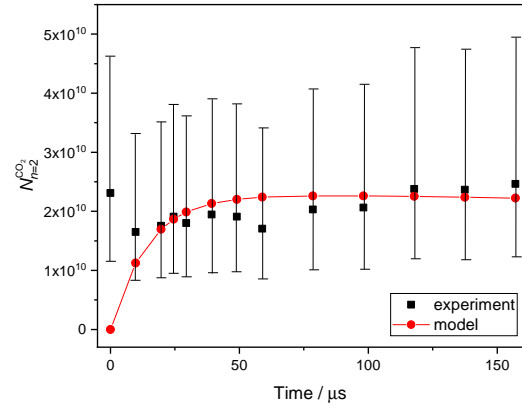
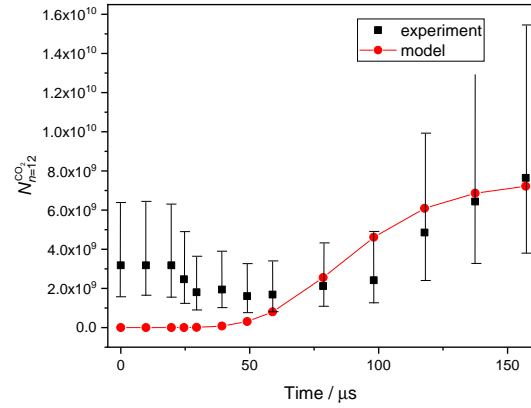


Figure S4: Concentration evolution of the dimer and the 8 or 12-mer as a function of the nucleation time for C_3H_8 . The experimental data points are shown as black squares and the simulated data is shown as red dots. The uncertainty of a factor of 2 is indicated by error bars.

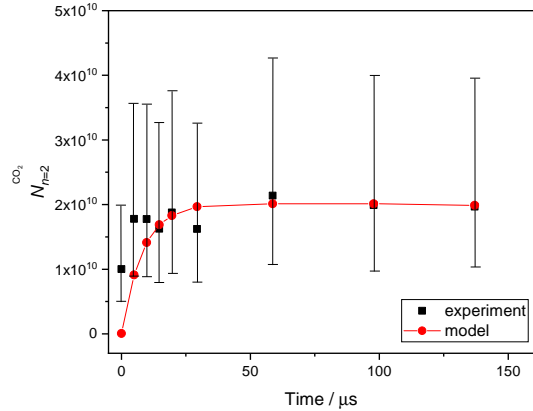
0.12 % CO₂ $n = 2$



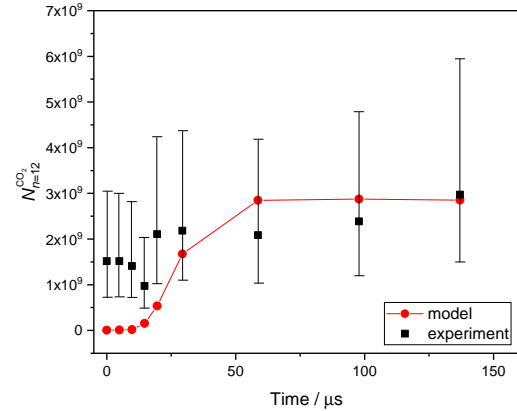
0.12 % CO₂ $n = 12$



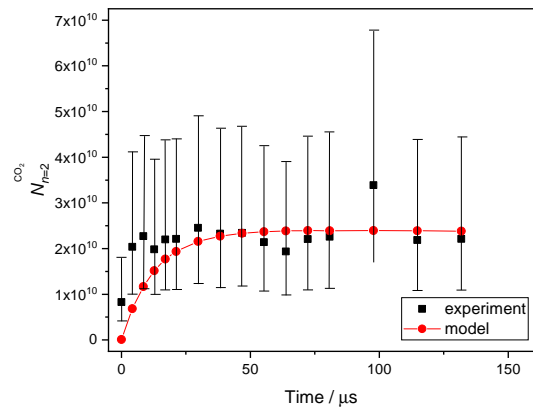
1.1 % CO₂ $n = 2$



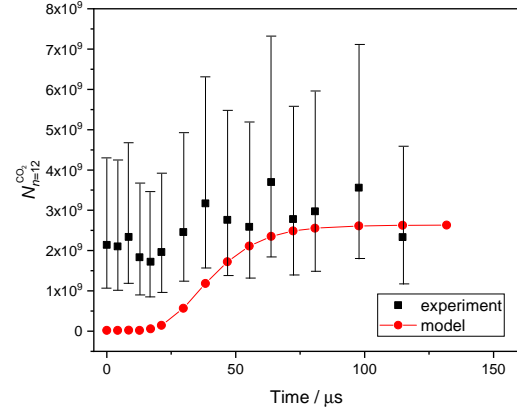
1.1 % CO₂ $n = 12$



3.3 % CO₂ $n = 2$



3.3 % CO₂ $n = 12$



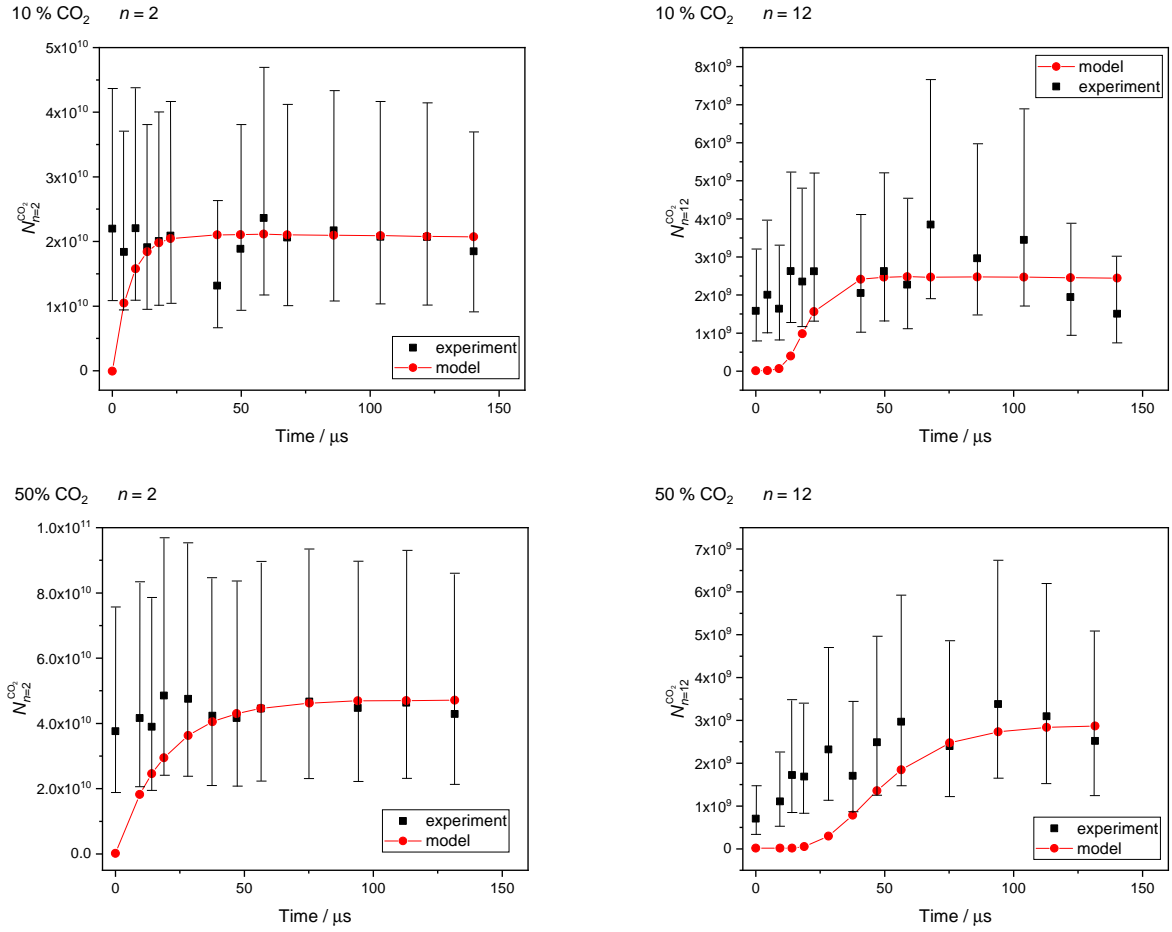


Figure S5: Concentration evolution of the dimer and the 12-mer as a function of the nucleation time for CO_2 . The experimental data points are shown as black squares and the simulated data is shown as red dots. The uncertainty of a factor of two is indicated by error bars.

49 **Enhancement model**

50 **Force Field model**

51 The interaction potential between a cluster and one approaching monomer unit is mod-
 52 eled with a Transferable Potentials for Phase Equilibria (TraPPE) force-field (FF). The FF
 53 parameters are given in Table S2 [11, 12].

fragment	σ	ϵ	q
C	2.80 Å	$2.3267 \cdot 10^{-3}$ eV	+0.70 e
O	3.05 Å	$6.8077 \cdot 10^{-3}$ eV	-0.35 e
CH ₃	3.75 Å	$8.4450 \cdot 10^{-3}$ eV	0
CH ₂	3.95 Å	$3.9640 \cdot 10^{-3}$ eV	0

Table S2: Force field paramters [11, 12].

54 Parameters for interactions between different fragments are calculated using the Lorentz-
 55 Berthelot combining rules:

$$\sigma_{ij} = \frac{\sigma_{ii} + \sigma_{jj}}{2}, \quad \epsilon_{ij} = \sqrt{\epsilon_{ii}\epsilon_{jj}} \quad (8)$$

56 The potential between a cluster and monomer for a certain center-of-mass distance (R) and
 57 orientation (Ω) is calculated by summing up all the pair-potential contributions between a
 58 fragment in the cluster (i) and one in the monomer (j):

$$V(R, \Omega) = \sum_i \sum_j 4\epsilon_{ij} \left[\left(\frac{\sigma_{ij}}{R_{ij}} \right)^{12} - \left(\frac{\sigma_{ij}}{R_{ij}} \right)^6 \right] + \frac{1}{4\pi\epsilon_0} \frac{q_i q_j}{R_{ij}} \quad (9)$$

59 R_{ij} is the center-of-mass distance between the fragments. As input, the structure of the cluster
 60 is necessary. The structures of (CO₂)_n clusters with n molecules have been calculated in our
 61 previous publication [13] and we use them here as input for the enhancement model. For
 62 propane only the monomer-monomer potential was evaluated. The fragments (CH₂, CH₃)
 63 in the propane monomer have a fixed bond length of 1.54 Å and a bond angle of 114° [12].
 64 We now introduce the orientationally averaged effective potential $V_{\text{eff}}(R)$, as a function of the
 65 intermolecular distance R [14]

$$V_{\text{eff}}(R) = \langle V(R, \Omega) \rangle_{\Omega} + \frac{E_T b^2}{\vec{R}^2} \quad (10)$$

66 b is the impact parameter, E_T is the relative translational energy and $V(R)$ is the orientationally
 67 averaged TraPPE (eq.9)

$$V(R) = \langle V(R, \Omega) \rangle_{\Omega} \quad (11)$$

⁶⁸ Let R_{\max} be the intermolecular distance at which $V_{\text{eff}}(R)$ is maximal.

$$\frac{d}{dR} \left(V(R) + \frac{E_{\text{T}} b^2}{R_{\max}^2} \right)_{R=R_{\max}} = 0 \quad (12)$$

⁶⁹ For a collision to take place E_{T} must exceed $V_{\text{eff}}(R_{\max})$, so that the following conditions determine the maximum impact parameter b_{\max} for which collision is possible:

$$E_{\text{T}} = V(R_{\max}) + \frac{E_{\text{T}} b_{\max}^2}{R_{\max}} \quad (13)$$

⁷¹ Solving eq.13 for b_{\max} and assuming a Maxwell distribution for the translational energy E_{T}

$$\chi(E_{\text{T}}) = 2 \left(\frac{1}{k_{\text{B}} T} \right)^{3/2} \sqrt{\frac{E_{\text{T}}}{\pi}} \exp \left(-\frac{E_{\text{T}}}{k_{\text{B}} T} \right) \quad (14)$$

⁷² yields the monomer-cluster association rate constants $k_{1j,\text{inter}}$:

$$k_{1j,\text{inter}} = \int_0^\infty \sqrt{\frac{2E_{\text{T}}}{m}} \pi b_{\max}^2 \chi(E_{\text{T}}) dE_{\text{T}} \quad (15)$$

⁷³ Finally, the theoretical enhancement factor η_{calc} can be determined with eq. 9 in the main text.

⁷⁴ ΔG_j^* for small CO₂ clusters as a function of T

⁷⁵ The values of reduced ΔG_j^* from the DFT calculations that were used for determining J_{QM}
⁷⁶ are given below in Table S3.

Table S3: $\Delta G_j^*(k_B T)^{-1}$ for CO₂ cluster sizes up to $j = 12$

j	31.2 K	44.4 K	49.3 K	56.6 K	62.9 K
2	80.77	52.12	45.77	38.50	33.68
3	148.78	96.38	84.82	71.64	62.91
4	200.87	130.23	114.76	97.16	85.53
5	253.64	165.09	145.82	123.95	109.54
6	302.85	196.67	173.64	147.52	130.34
7	343.64	223.33	197.38	168.07	148.81
8	388.88	252.31	222.94	189.76	167.99
9	434.24	281.39	248.57	211.55	187.26
10	486.14	315.23	278.56	237.20	210.08
11	522.52	338.40	299.01	254.65	225.59
12	558.78	360.68	318.38	270.76	239.58

⁷⁷ Fig. S6 shows ΔG_j , the free energy of formation at the experimental supersaturation (NOT
⁷⁸ at $S = 1$, therefore without asterisk). This exemplifies the emergence of a nucleation barrier
⁷⁹ with increasing flow temperature. Note that the calculations still predict a small energy barrier
⁸⁰ for the coldest temperature; however, this barrier vanishes with a variation of ΔG_j by a few
⁸¹ percent. Therefore, it lies within the uncertainty of the calculations as discussed in the next
⁸² section.

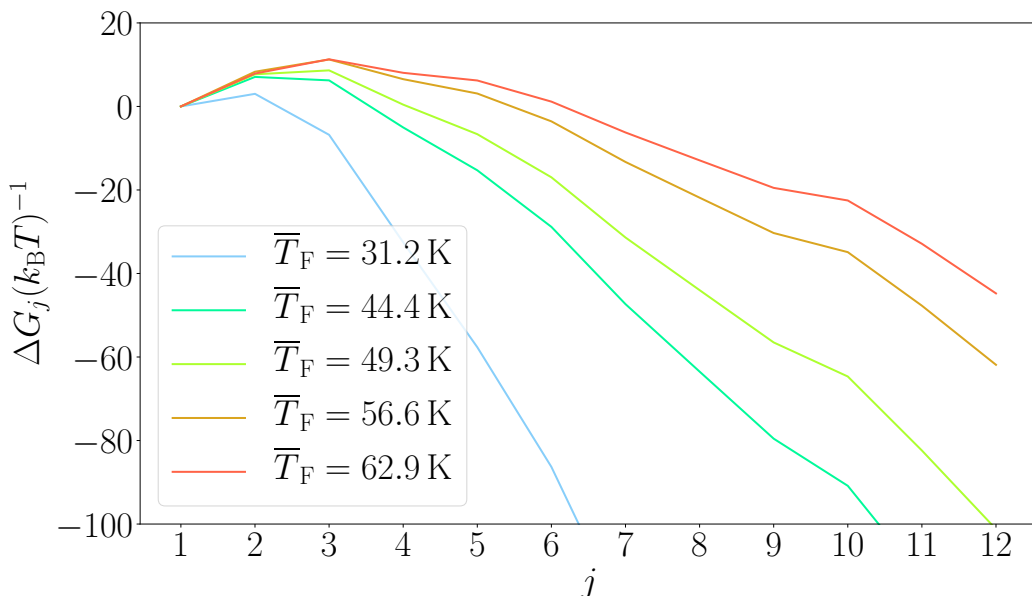


Figure S6: $\Delta G_j(k_B T)^{-1}$ from DFT calculations for the five experimental temperatures as a function of cluster size j .

83 **Sensitivity analysis of ΔG_j^* and J_{QM}**

84 Lemke and Seward [15] compared different DFT calculations with different functionals and
 85 basis sets with CCSD(T) level calculations and showed that M06-2X is a good functional to
 86 describe the interactions in $(\text{CO}_2)_n$ clusters. However, the calculations do have limitations
 87 which leads to a small error in ΔG_j^* . J_{QM} uses the calculated ΔG_j^* values as input, see eq. 15 in
 88 the main text. As ΔG_j^* is in the exponent of the formula, already minor errors on ΔG_j^* lead to
 89 large errors in J_{QM} . In Table S4, we assume an uncertainty of 5% on ΔG_j^* and show the effect
 90 on J_{QM} .

Table S4: Nucleation rate J_{QM} for variations of ΔG_j^* by $\pm 5\%$.

	31.2 K	44.4 K	49.3 K	56.6 K	62.9 K
95% ΔG_j	$4.1 \cdot 10^{17}$	$5.9 \cdot 10^{17}$	$8.6 \cdot 10^{17}$	$7.6 \cdot 10^{17}$	$1.2 \cdot 10^{19}$
100% ΔG_j	$4.7 \cdot 10^{16}$	$3.3 \cdot 10^{16}$	$3.5 \cdot 10^{16}$	$2.6 \cdot 10^{16}$	$5.4 \cdot 10^{17}$
105% ΔG_j	$9.1 \cdot 10^{14}$	$7.5 \cdot 10^{14}$	$6.8 \cdot 10^{14}$	$7.4 \cdot 10^{14}$	$2.1 \cdot 10^{16}$

91 The nucleation rate J_{QM} can change by up to two orders of magnitude with a minor change
 92 in ΔG_j^* . At high temperatures J_{QM} is more sensitive to an increase of ΔG_j^* (+5%), while
 93 at lower temperatures it is more sensitive to a decrease in ΔG_j^* (-5%). These variations can
 94 only give an estimate for some of the uncertainties affecting J_{QM} . Additional uncertainties
 95 arise from the calculated structure of the clusters and from the calculated hard sphere collision
 96 rates. However, these contributions are difficult to quantify. As a rough estimate, we quote an
 97 uncertainty of \pm two orders of magnitude for the values we determine for J_{QM} .

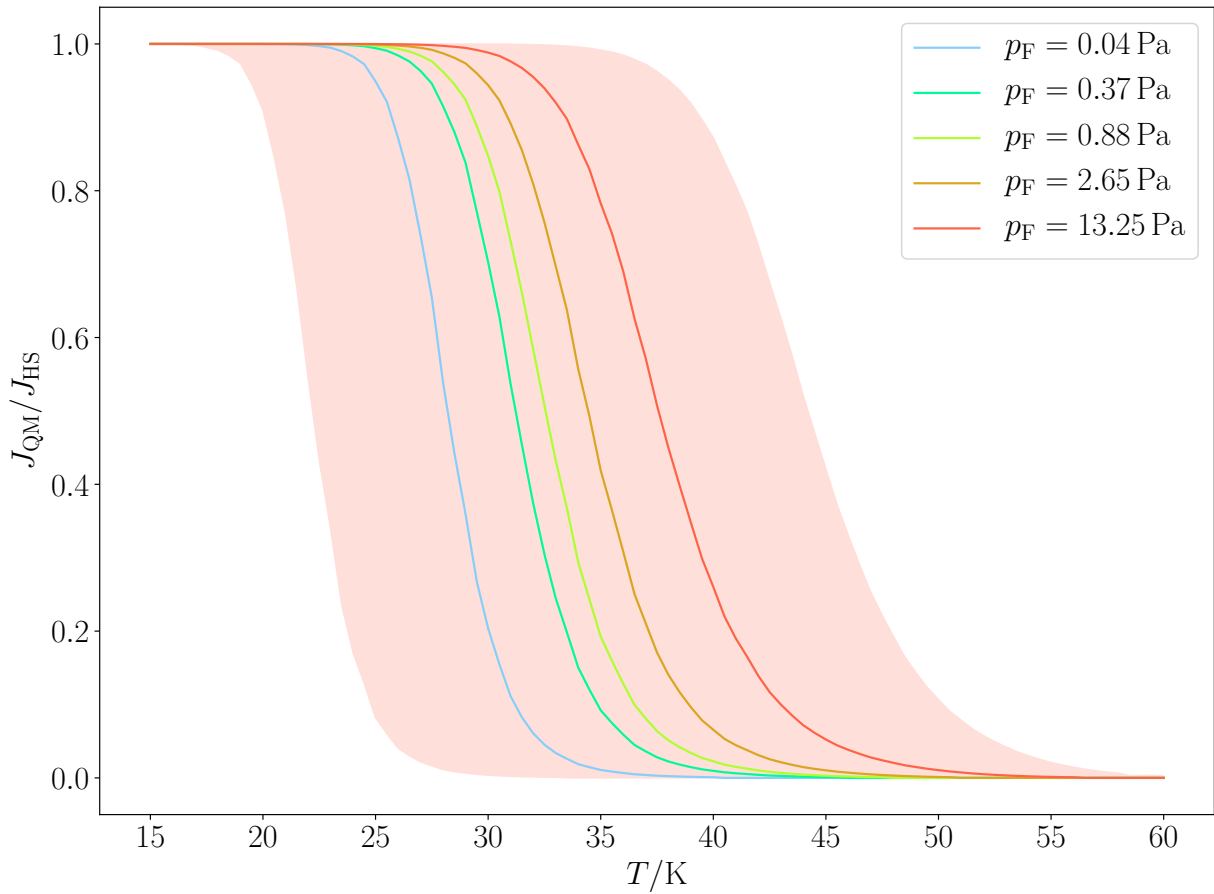


Figure S7: Ratio of J_{QM} to J_{HS} as a function of temperature for the five experimental partial pressures of CO₂.

As mentioned in section 4.4 in the main text, J_{QM} quickly approaches J_{HS} below a certain temperature. This transition is shown in Fig. S7 for the five partial pressures of CO₂ from the experiment. The red shaded area indicates the uncertainty resulting from a variation of ΔG_j^* by 5% as discussed above. At a pressure of $p_F = 0.04$ Pa J_{QM} reaches 90% of the hard sphere limit J_{HS} at a temperature of 25.8 K. Upon variations of ΔG_j^* by 5% this temperature varies from 20.1 K to 30.8 K, the latter lying close to the experimental value of 31.2 K.

¹⁰⁴ **Coordinates for CO₂ clusters from DFT calculations**

¹⁰⁵ Here, the structures calculated in [13] were used as input parameters and then further refined
¹⁰⁶ with a larger basis set (aug-cc-pVTZ). This was done in order to improve the accuracy of ΔG_j^*
¹⁰⁷ for the calculation of J_{QM} . The changes in structure of the (CO₂)_j clusters are minor. The
¹⁰⁸ coordinates of the CO₂ clusters are given in the following.

Table S5: CO₂ monomer structure

atom	x	y	z
C	0.00000	0.00000	0.00000
O	0.00000	0.00000	1.15531
O	0.00000	0.00000	-1.15531

Table S6: (CO₂)₂ structure

atom	x	y	z
C	-1.67003	-0.28355	0.00002
O	-2.41823	0.59418	-0.00078
O	-0.92491	-1.16935	0.00079
C	1.67003	0.28353	-0.00001
O	2.41757	-0.59474	-0.00080
O	0.92558	1.16992	0.00078

Table S7: (CO₂)₃ structure

atom	x	y	z
C	-0.54585	2.16815	0.00060
O	0.50387	1.68123	-0.00018
O	-1.58319	2.67141	0.00136
C	2.15099	-0.61133	0.00085
O	3.10463	0.03678	-0.00286
O	1.20574	-1.27891	0.00380
C	-1.60543	-1.55662	-0.00142
O	-1.70896	-0.40410	-0.00279
O	-1.52187	-2.70655	0.00064

Table S8: $(CO_2)_4$ structure

atom	x	y	z
C	1.03106	2.10031	0.06586
O	-0.05099	1.68917	0.12385
O	2.09765	2.53113	0.01502
C	-0.77479	-0.52368	1.80341
O	-1.89444	-0.24288	1.77588
O	0.34552	-0.80604	1.84108
C	-1.89323	-0.04948	-1.22811
O	-2.68044	0.77195	-1.40588
O	-1.10655	-0.88392	-1.06104
C	1.63571	-1.52864	-0.63964
O	1.37854	-2.64328	-0.49624
O	1.91165	-0.41502	-0.79381

Table S9: $(CO_2)_5$ structure

atom	x	y	z
C	0.02776	2.17861	-0.43525
O	-0.64957	2.81543	-1.11407
O	0.72977	1.55547	0.24493
C	-0.76974	-1.39108	-1.45496
O	-0.87370	-0.23869	-1.53063
O	-0.67354	-2.53658	-1.39599
C	0.64654	-0.77392	1.79589
O	-0.38776	-1.06656	1.36769
O	1.67627	-0.49680	2.23566
C	-2.75919	0.21698	0.61191
O	-2.30212	1.22843	0.93570
O	-3.22645	-0.78895	0.29144
C	2.85275	-0.23028	-0.51315
O	3.68625	0.54173	-0.32518
O	2.02225	-1.01373	-0.71288

Table S10: $(CO_2)_6$ structure

atom	x	y	z
C	-1.43716	2.27067	-0.07348
O	-1.59082	1.26547	0.48318
O	-1.30221	3.27929	-0.61159
C	-2.27339	-1.43542	0.07750
O	-1.26996	-1.59133	-0.48185
O	-3.28027	-1.29852	0.61837
C	-0.00220	0.00530	-2.40629
O	0.90618	-0.70828	-2.42094
O	-0.91078	0.71877	-2.41564
C	2.27287	1.43729	0.07857
O	1.26807	1.59375	-0.47808
O	3.28109	1.29977	0.61674
C	0.00293	-0.00594	2.40663
O	-0.71005	-0.91487	2.41659
O	0.71592	0.90290	2.42054
C	1.43703	-2.27168	-0.08312
O	1.30063	-3.27900	-0.62336
O	1.59215	-1.26813	0.47619

Table S11: $(CO_2)_7$ structure

atom	x	y	z
C	-2.90904	0.97595	-0.08202
O	-2.27688	0.66574	0.84104
O	-3.54651	1.29564	-0.98417
C	1.72951	-2.45925	-0.14967
O	1.40853	-2.28763	-1.24711
O	2.04683	-2.64205	0.94530
C	-0.12324	2.74866	0.51459
O	-0.45524	2.62085	-0.58702
O	0.18543	2.88138	1.61819
C	-2.09700	-2.17391	0.08985
O	-1.06893	-2.36947	0.58340
O	-3.12900	-1.99016	-0.39113
C	3.05341	1.03567	-0.29322
O	3.46559	-0.03894	-0.39013
O	2.65782	2.11598	-0.18451
C	0.05936	0.11577	-1.94833
O	1.09054	0.54452	-2.23355
O	-0.98291	-0.31021	-1.67924
C	0.29341	-0.24715	1.86090
O	0.70959	0.03767	0.81371
O	-0.10968	-0.52013	2.90115

Table S12: $(CO_2)_8$ structure

atom	x	y	z
C	-1.04417	2.67578	-0.57812
O	-1.64282	2.52429	0.40117
O	-0.46777	2.82921	-1.56544
C	3.96760	-0.16078	-1.04561
O	3.07541	0.45950	-1.44795
O	4.86704	-0.76402	-0.65284
C	-3.52826	0.41550	-0.65014
O	-4.44684	0.60309	0.01628
O	-2.61084	0.23635	-1.33864
C	-1.10059	0.16711	2.02850
O	-1.93258	-0.45612	1.51957
O	-0.28179	0.78865	2.55015
C	1.46893	-2.03157	0.94614
O	2.12829	-2.11739	0.00042
O	0.81136	-1.95902	1.89223
C	0.29689	-0.14856	-1.49419
O	0.31148	-0.47573	-2.59447
O	0.27497	0.18402	-0.38044
C	-2.11367	-2.51641	-0.39185
O	-0.96817	-2.51443	-0.55532
O	-3.25701	-2.53163	-0.24040
C	2.05679	1.59397	1.19407
O	2.60873	0.62814	1.51314
O	1.52791	2.56879	0.87594

Table S13: $(CO_2)_9$ structure

atom	x	y	z
C	0.02722	-0.43071	-1.36272
O	-0.00418	-0.28239	-0.21150
O	0.06341	-0.59051	-2.50019
C	3.34197	-1.81399	-0.73386
O	3.88507	-2.78897	-0.45426
O	2.81115	-0.82274	-1.01985
C	-3.19790	-1.86009	-0.86804
O	-4.27988	-1.46957	-0.78731
O	-2.11803	-2.26692	-0.95846
C	-0.03543	3.24220	0.63051
O	-0.93049	2.50919	0.59992
O	0.84319	3.98853	0.66166
C	-1.56873	0.03281	2.01504
O	-2.51198	-0.16622	1.37715
O	-0.64136	0.23744	2.67107
C	-3.19173	1.48091	-0.89021
O	-3.92324	2.13173	-0.28386
O	-2.46327	0.83347	-1.51732
C	0.08204	-2.89994	0.78638
O	-0.62849	-2.69423	1.67286
O	0.79277	-3.12096	-0.09847
C	2.58874	2.11505	-1.22263
O	3.69945	2.24960	-0.94699
O	1.47461	1.98448	-1.51217
C	1.95058	0.13306	1.65043
O	1.90560	1.26449	1.42060
O	2.02806	-0.99592	1.88345

Table S14: $(CO_2)_{10}$ structure

atom	x	y	z
C	3.33130	1.08900	-0.04573
O	2.76904	0.52813	-0.88953
O	3.90549	1.65210	0.77833
C	0.04453	-0.03982	-1.18333
O	0.09841	0.41638	-2.23895
O	-0.01869	-0.50286	-0.12238
C	0.57002	3.34023	-1.73158
O	1.17946	3.03249	-0.79538
O	-0.02600	3.66227	-2.66287
C	-0.41565	-3.26095	-0.23790
O	-1.13387	-3.05500	-1.12001
O	0.29973	-3.48292	0.64081
C	-3.52327	-1.46821	-1.18467
O	-2.90547	-0.49324	-1.06511
O	-4.15323	-2.42325	-1.30467
C	1.44931	-1.27294	2.10302
O	2.41167	-1.27087	1.46286
O	0.50157	-1.28249	2.76197
C	-2.68658	2.15568	-0.09416
O	-3.77310	2.20270	0.28426
O	-1.59621	2.11743	-0.48370
C	2.99622	-2.20709	-1.30820
O	4.11177	-2.18802	-1.02015
O	1.88009	-2.24398	-1.61480
C	-2.04770	-0.70477	1.77887
O	-1.91275	0.42081	2.00343
O	-2.21683	-1.82565	1.55639
C	0.28338	2.36692	1.90693
O	1.03574	1.49676	1.78615
O	-0.45798	3.24066	2.04090

Table S15: $(CO_2)_{11}$ structure

atom	x	y	z
C	1.49375	-3.07304	-0.46319
O	1.18905	-3.50256	0.56423
O	1.80443	-2.65765	-1.49639
C	-3.42388	0.17789	-2.24699
O	-3.53003	1.31427	-2.06655
O	-3.33884	-0.95801	-2.43771
C	-1.58387	3.11632	-0.87938
O	-1.39406	3.57895	-1.91661
O	-1.77456	2.66908	0.17281
C	0.10797	2.11975	2.35518
O	-0.40906	1.08480	2.33028
O	0.61897	3.15266	2.39622
C	-0.08535	-0.05405	-0.87024
O	-0.63301	0.37735	-1.78866
O	0.47176	-0.48417	0.04829
C	-2.95314	0.18469	1.40663
O	-3.35566	0.54755	2.42125
O	-2.56871	-0.18404	0.37662
C	3.54630	-0.47830	-2.10603
O	2.75445	0.28731	-1.74096
O	4.34392	-1.22128	-2.47317
C	-2.29019	-2.84631	-0.44513
O	-3.31172	-3.07227	0.03765
O	-1.26225	-2.63790	-0.93620
C	2.96506	-0.19723	1.21178
O	2.64235	0.84172	1.60162
O	3.31790	-1.22279	0.81388
C	2.21347	2.75644	-0.47174
O	3.31918	3.07735	-0.46705
O	1.09843	2.44221	-0.48301
C	0.01111	-1.71019	2.51071
O	1.09044	-1.47424	2.84601
O	-1.07388	-1.95531	2.19627

Table S16: $(CO_2)_{12}$ structure

atom	x	y	z
C	2.87659	-1.01736	1.43582
O	1.94771	-0.32320	1.47382
O	3.80192	-1.69942	1.41305
C	-3.08282	1.12846	-1.86816
O	-4.00944	1.74308	-1.56713
O	-2.15894	0.50754	-2.18753
C	-1.29099	-2.15909	-2.56098
O	-2.30605	-2.50950	-2.13858
O	-0.27915	-1.80921	-2.99897
C	-2.91756	-1.85925	0.72140
O	-2.42116	-2.86414	0.99657
O	-3.43263	-0.85802	0.45599
C	0.03064	0.07061	-0.48671
O	0.60478	1.02754	-0.78771
O	-0.53131	-0.89411	-0.19492
C	-2.43353	1.68175	1.61867
O	-1.91487	1.70177	0.58102
O	-2.95720	1.68193	2.64255
C	-0.54773	3.66633	-0.94260
O	-1.17355	3.38131	-1.86998
O	0.07185	3.96985	-0.01560
C	1.43797	2.34833	1.84613
O	0.44383	2.05111	2.35673
O	2.44042	2.64474	1.35698
C	0.36657	-3.44365	0.39095
O	0.75178	-3.05265	1.40907
O	-0.00469	-3.85057	-0.62277
C	2.51143	-1.40550	-2.20401
O	2.83934	-1.00770	-3.23313
O	2.18337	-1.80482	-1.16620
C	-0.18087	-0.87572	3.30085
O	0.66733	-1.12240	4.04167
O	-1.04460	-0.62636	2.57188
C	3.23306	1.86223	-1.25108
O	2.86412	2.86863	-1.67293
O	3.61506	0.84674	-0.84410

¹⁰⁹ **References**

- ¹¹⁰ [1] Verein deutscher Ingenieure and Gesellschaft Verfahrenstechnik und Chemieingenieurwesen, *VDI-Wärmeatlas*, Springer Vieweg (2013).
- ¹¹¹
- ¹¹² [2] National Institute of Standards and Technology <http://webbook.nist.gov/chemistry/>
- ¹¹³ [3] W. F. Giauque and C. J. Egan, *J. Chem. Phys.*, **5**, 45-54 (1937).
- ¹¹⁴ [4] J. H. Dymond, K. N. Marsh, R. C. Wilhoit, K. C. Wong, *Virial Coefficients of Pure Gases and Mixtures. Vol. 21*, Springer-Verlag (2002).
- ¹¹⁵
- ¹¹⁶ [5] M. Lippe, S. Chakrabarty, J. J. Ferreiro, K. K. Tanaka and Ruth Signorell *J. Chem. Phys.*, **149**, 244303 (2018).
- ¹¹⁷
- ¹¹⁸ [6] M. Azreg-Ainou, *Monatsh. Chem.*, **136**, 2017-2027 (2005).
- ¹¹⁹ [7] R. A. Perkins, J. C. Sancheu Ochoa, J. W. Magee, *J. Chem. Eng. Data*, **54**, 12, 3192-3201 (2009).
- ¹²⁰
- ¹²¹ [8] J. D. Kemp, C. J. Egan, *J. Am. Chem. Soc.*, **60**, 1521-1525 (1938).
- ¹²² [9] S. Salerno, M. Cascella, D. May, P. Watson, D. Tassios, *Fluid Phase Equilib.*, **27**, 15-34 (1986).
- ¹²³
- ¹²⁴ [10] C. Li, M. Lippe, J. Krohn and R. Signorell *J. Chem. Phys.*, **151**, 094305 (2019).
- ¹²⁵ [11] J. J. Potoff and J. I. Siepmann, *AIChE J.*, **47**, 1676-1682 (2001).
- ¹²⁶ [12] M. G. Martin and J. I. Siepmann, *J. Phys. Chem. B*, **102**, 2569-2577 (1998).
- ¹²⁷ [13] M. Lippe, U. Szczepaniak, G.-H. Hou, S. Chakrabarty, J. J. Ferreiro, E. Chasovskikh and R. Signorell, *J. Phys. Chem. A*, **123**, 2426-2437 (2019).
- ¹²⁸
- ¹²⁹ [14] R. D. Levine and R. B. Bernstein, *Molecular reaction dynamics and chemical reactivity*, Oxford University Press (1987).
- ¹³⁰
- ¹³¹ [15] K. H. Lemke, T. M. Seward, *Chem. Phys. Lett.*, **573**, 19-23 (2013).